

Static and Dynamic Spectroscopy of (Al,Ga)As/GaAs Microdisk Lasers with Interface Fluctuation Quantum Dots

W.H. Wang¹, S. Ghosh², F. M. Mendoza², X. Li¹, D. D. Awschalom², and N. Samarth^{1,2*}

¹ *Materials Research Institute, Penn State University, University Park PA 16802*

² *Center for Spintronics and Quantum Computation,
University of California, Santa Barbara CA 93106*

(Dated: October 30, 2019)

Abstract

We have studied the steady state and dynamic optical properties of semiconductor microdisk lasers wherein whispering gallery cavity modes are coupled to the emission from interface fluctuation quantum dots in GaAs/(Ga,Al)As quantum wells. Steady-state measurements of the stimulated emission yield a quality factor $Q \sim 6200$ and a coupling constant $\beta \sim 0.09$. The broad gain spectrum produces mode hopping between spectrally adjacent whispering gallery modes as a function of temperature and excitation power. Time- and energy-resolved photoluminescence measurements show that the emission rise and decay rates increase significantly with excitation power. Marked differences are observed between the radiative decay rates in processed and unprocessed samples.

PACS numbers: 03.67.Lx, 42.55.Sa, 78.47.+p, 78.67.Hc

Current interest in quantum information processing has motivated several fundamental studies of the coupling between zero dimensional (0D) electronic states and confined photon modes in semiconductor microdisks.^{1,2,3} These experiments have focused on high finesse microdisks where the 0D states of self-assembled InAs quantum dots (QDs) couple with the whispering gallery modes (WGMs) of a cylindrical microcavity, and are characterized by a large coupling constant ($\beta \sim 0.1$) between the spontaneous emission and the cavity modes. Due to the large gain width created by the spectrally broad QD emission, such microdisks exhibit simultaneous stimulated emission from several whispering gallery cavity modes.³ This behavior contrasts with microdisks containing two-dimensional (2D) quantum well (QW) states that typically show stimulated emission from a single cavity mode due to the narrower gain width, but suffer from lower Q (typically between ~ 3000 and ~ 5000) because of larger absorption in the QW.^{4,5} Here, we discuss the spontaneous and stimulated emission from microdisks that lie in an intermediate regime, where the active region contains interface fluctuation quantum dots (IFQDs) within narrow GaAs quantum wells.⁶ This design drastically reduces the number of modes that lase simultaneously, while allowing for a relatively high Q -factor ($Q \sim 6200$) and large coupling constant ($\beta \sim 0.09$) due to the interaction between 0D states and cavity modes. We note that although recent experiments have studied triggered single photon emission from IFQDs incorporated into patterned disks, we are unaware of any demonstrated mode coupling and/or stimulated emission in such structures.⁷

The microdisks in this study are patterned from GaAs/(Ga,Al)As heterostructures grown by molecular beam epitaxy (MBE) on (001) semi-insulating GaAs substrates. The samples consist of a 120 nm thick GaAs buffer layer, a 500 nm thick $\text{Al}_{0.8}\text{Ga}_{0.2}\text{As}$ pedestal layer, and finally a 110 nm thick $\text{Al}_{0.31}\text{Ga}_{0.69}\text{As}/\text{GaAs}$ heterostructure that forms the microdisk itself. The microdisk region contains an optically active region with six 4.2 nm thick GaAs QWs, isolated from each other by 10 nm thick $\text{Al}_{0.31}\text{Ga}_{0.69}\text{As}$ barriers. This optically active region is sandwiched between 38 nm thick $\text{Al}_{0.31}\text{Ga}_{0.69}\text{As}$ layers. At each interface, growth interruptions of 30 seconds are used to induce IFQDs. We also fabricate control samples with the optically active region containing either 10 nm wide QWs or 4.2 nm QWs with no growth interruption. In the former, the confined electronic states are explicitly 2D, while in the latter the density and extent of the lateral 0D confining region is highly reduced. As discussed elsewhere,⁸ low temperature micro-photoluminescence measurements show clear

resolution-limited spectral features only in the samples with growth interruptions.

Microdisks are processed from the MBE-grown wafers using standard photolithography procedures, followed by a two-step HBr and $(\text{NH}_4)_2\text{S}$ wet chemical etch, described in detail elsewhere.⁸ In the first step, a nonselective HBr-based mesa etch defines the circular portion of the microdisk. The $(\text{NH}_4)_2\text{S}$ etch serves a dual purpose: it passivates the surface states,⁴ and also etches the $\text{Al}_{0.8}\text{Ga}_{0.2}\text{As}$ layer with high selectivity, producing microdisks of $\sim 4\mu\text{m}$ diameter on narrow pedestals (Fig. 1(a)). Finally, we stabilize the sulfide layers by encapsulating the sample with 40 nm SiN_x deposited using electron cyclotron resonance plasma enhanced chemical vapor deposition.

We perform steady-state photoluminescence (PL) measurements using continuous wave (CW) 568 nm excitation from an Ar/Kr mixed gas laser. The samples are mounted on a cold finger in a liquid He continuous flow cryostat, with a temperature sensor co-mounted on the cold finger close to the sample to monitor heating effects. Both the optical excitation and collection use an objective lens (100X, numerical aperture 0.73) with an excitation spot diameter of 20 μm ; the collected PL is spectrally resolved by a monochromator (spectral resolution = 180 μeV) and detected by a LN2 cooled charge coupled device detector. Polarization-resolved PL measurements are carried out in the far field in a different optical cryostat. Time-resolved PL measurements are carried out using similar excitation/collection optics, but the optical pumping is carried out with a pulsed Ti-Sapphire laser at 740 nm (repetition rate of 76 MHz and pulse width of 150 fs). The PL is then temporally resolved using a streak camera, which is phase-locked to the pulsed laser in order to synchronize the sweep pulse of the streak tube with the incoming signal. The time resolution of the streak camera is 2 ps.

Figure 1(b) shows the CW emission spectra of a single microdisk laser for three different excitation powers. At the lowest excitation power, the spontaneous emission dominates the spectrum, but we already see evidence for the coupling of the PL emission to a few cavity modes (identified later as WGMs). As the power increases, one of the WGMs lases, with the onset of lasing defined by a clear threshold (Fig. 1(c)). We note that the intensity of the integrated PL continues to increase above the lasing threshold; this contrasts with the carrier pinning effect observed in conventional semiconductor lasers and is probably due to the non-equilibrium heating of the gain medium, as has been reported in other high coupling constant microdisks.^{9,10}

Because it is not possible to obtain an exact analytical solution for the modes of a cylindrical dielectric slab, we use a well-known approximation that treats the problem as a guided wave with vacuum wavelength λ traveling along the axial direction (z) of a dielectric slab waveguide of refractive index n_{eff} , thickness D and radius R .¹¹ The resulting eigenfrequencies are characterized by a set of three mode numbers (m, l, p) corresponding to the azimuthal, radial and planar degrees of freedom, respectively. We ignore the planar mode number p because only the lowest order planar mode ($p = 0$) in the z direction is allowed by the thin microdisk ($D/\lambda \sim 0.14$). We estimate the refractive index in the axial direction (n_z) from $\tan\left[\frac{k_z D}{2}\right] = \frac{h}{k_z}$, where k_z is the wave vector in the z direction, and $k_z^2 + h^2 \equiv k^2 [n_1^2 + n_2^2]$, with n_1 and n_2 being the refractive indices inside and outside the disk structure respectively. The effective index in the azimuthal direction is then calculated from $n_{\text{eff}} = \alpha \sqrt{n_1^2 - n_z^2}$, $\alpha = f - \frac{g}{R/\lambda}$ with parameters $f = 0.984$, $g = 0.163$ for $l = 1$.¹¹ This results in $n_{\text{eff}} \sim 2.3$, compared to the bulk value $n = 3.4$. We then use this value of n_{eff} to estimate the allowed eigenfrequencies by solving the two dimensional Helmholtz equation, whose solution results in Bessel functions of the first kind.¹² This calculation identifies the laser emission at 1.61 eV as a WGM with TE polarization and $m = 35, l = 1$. The far field laser emission collected from the side of the microdisk is strongly polarized in the disk plane (Fig. 1(d)), confirming the TE nature of the stimulated emission. We note that selection rules for recombination between conduction band electrons and heavy holes also produce the same polarization for spontaneous emission in this geometry, suggesting a possible reason for the preferred coupling of the emission to a TE rather than a TM cavity mode.

Figure 2(a) shows a log-log plot of the the laser emission intensity in this mode as a function of the excitation intensity I . The laser threshold (~ 240 W/cm²) is indicated by a kink in this plot, highlighted by the arrow. (As a comparison, we note that microdisks patterned from the 4.2 nm and 10 nm QW control samples exhibit somewhat higher thresholds of 410 W/cm² and 300 W/cm², respectively.) The laser emission intensity is proportional to the photon number p in the mode, which we define as unity at the threshold.¹³ To determine the cavity coupling constant β , we fit the data in Fig. 2(a) using the following equation which relates the photon number to the excitation intensity:¹⁴

$$I(p) = A \left[\frac{p}{1+p} (1 + \xi)(1 + \beta p) - \xi \beta p \right]. \quad (1)$$

Here, the scale factor $A = \hbar \omega \gamma / \delta \beta$, where ω is the frequency of the mode, γ is the

cavity decay rate, and δ is the photon conversion efficiency. The dimensionless parameter ξ is defined by $\xi = N_0\beta V/\gamma\tau_{\text{sp}}$, where N_0 is the transparency carrier concentration of the gain material, V is the volume of the active material and τ_{sp} is the spontaneous emission lifetime. The above equation assumes that only one mode lases within the gain region, and that non-radiative recombination is negligible. Since we do not have direct knowledge of several parameters such as γ , N_0 and δ , we treat β , ξ and A as fitting parameters; the first two determine the shape of the function $I(p)$, while the latter only scales its overall magnitude. Our fits yield a coupling constant $\beta \sim 0.09$ and $\xi \sim 7$.¹⁵ For comparison, we also plot the theoretical curves expected for $\beta = 1, 0.1, 0.01$. In a conventional laser where $\beta \sim 10^{-3}$, the photon number typically undergoes a sudden jump at threshold. Because of the high coupling constant of the cavity, the output power in these microdisk lasers increases with a finite slope around the transition region as shown in Fig. 2(a).

Figure 2 (b) shows the power dependence of the energy and the full width at half maximum (FWHM) of the $\text{TE}_{35,1}$ laser mode. For pump power below 0.4 kW/cm^2 , the peak energy undergoes a blue shift with increasing pump power because the refractive index decreases with increasing carrier density.¹⁶ However, the plateau in the peak energy between 0.4 kW/cm^2 and 1.4 kW/cm^2 indicates that the blue shift is offset by local heating of the microdisk, eventually resulting in a red shift at the highest excitation densities. Figure 2(b) also shows that the FWHM undergoes an anomalous linewidth enhancement in the threshold region ($P \sim 240 \text{ W/cm}^2$). The coupling between refractive index fluctuations and the carrier fluctuations in the gain medium may explain this broadening.¹⁰ Below the threshold, the linewidth follows the standard Schawlow-Townes formula. Above the threshold, the linewidth is inversely proportional to output power and is described by a modification of this formula, wherein the linewidth is multiplied by a factor $(1 + \alpha^2)/2$, where α is the gain-refractive index coupling factor. The narrowest linewidth at $P \sim 55 \mu\text{W}$ is 0.26 meV while the emission wavelength is 1.61 eV , yielding an estimated $Q = \frac{E}{\Delta E} \sim 6200$ for this mode. In comparison, the control samples with 4.2 nm and 10 nm QWs yield $Q \sim 4000$ and 4500 , respectively.

The temperature dependence of the emission spectra is measured in the range $6\text{K} \leq T \leq 70\text{K}$ with a fixed CW excitation of 1.8 kW/cm^2 . Figure 2(c) shows that at high temperatures (between 50 K and 70 K), the laser emission cascades toward lower energies via three adjacent WGMs located between 1.61 eV and 1.59 eV (identified as $\text{TE}_{35,1}$, $\text{TE}_{30,2}$ and

TE_{26,3}, respectively). Note that in spectra (1) and (2) of Fig. 2(c), the emission intensity of the TE_{35,1} mode undergoes an abrupt transition toward the TE_{30,2} mode, without exciting the higher order mode located in between. We attribute the observed mode switching to a combination of effects: the temperature dependence of the gain profile, narrowing of the bandgap and possibly the thermal excitation of electrons/holes from deeply confined 0D states to shallower QW states. We also observe mode hopping at low temperatures when the excitation power is large compared to the single-mode operation region discussed earlier (Fig. 2(d)). Although the power-dependent mode hopping at low temperatures is also likely due to local heating of the microdisk (no changes are observed in the temperature sensor), we note that the transition from the TE_{35,1} to the TE_{30,2} mode is gradual, contrasting with the temperature-dependent changes shown in Fig. 2(c). We attribute this difference to the continued occupation of the 0D states at low temperatures as the pump power increases, as opposed to being depleted to higher states in fixed power/variable temperature measurements. Therefore, the TE_{35,1} mode does not quench completely and the high carrier density can sustain multiple-mode operation.

Time-integrated measurements of the microdisk emission using pulsed excitation show behavior that is similar to that obtained with CW excitation. In addition, we have measured the temporally and spectrally resolved emission spectra at different excitation powers (Fig. 3(a)). Both the rise and decay of the emission become faster as the pump power exceeds the threshold (190 W/cm² for this particular microdisk). This is shown in Fig. 3(b) where the decay and delay time is plotted as a function of pump power. The decay time, defined as the 1/eth time constant of the decay tail, is determined from exponential fits to the data. The delay (or rise) time is defined as the interval between the peaks of the excitation and microdisk emission pulses (arrow in Fig. 3(a)). The fast rise and decay dynamics is due to the increased stimulated emission rate which is proportional to the photon number in the cavity mode and which dominates the emission spectra above the lasing threshold. A qualitatively similar temporal characteristic has been reported in earlier, spectrally-integrated dynamical studies of GaAs/(Ga,Al)As microdisk QW lasers.⁵ In contrast to the shortening cavity-photon lifetime as the pump power increases, the photon lifetime in the unprocessed IFQD sample is power independent due to the lack of stimulated emission, as shown in Fig. 3(c).

Finally, we comment briefly on a comparison between the dynamical behavior of the microdisk with IFQDs and the control sample with 10 nm QWs. The pump-power depen-

dence of the spectrally- and time-resolved emission from the QW sample yields delay and decay times that are roughly identical to those observed for the IFQD sample. However, we note that the *spectrally-integrated* time-resolved emission does show apparent differences for the two types of samples: while the IFQD sample exhibits a single peak in the time domain, the QW sample shows a second peak that appears for high pump power after a delay of $\sim 200 - 300$ ps. The latter behavior is similar to that reported in previous spectrally-integrated studies of GaAs/(Ga,Al)As microdisk QW lasers where it was ascribed to carrier diffusion to the edges of the microdisk.⁵ However, the absence of such a peak in our spectrally-resolved measurements suggests that a different interpretation may be necessary since this peak does not appear at the same energy as the principal microdisk emission. A more detailed discussion of this phenomenon is beyond the scope of this manuscript and will be reported elsewhere.

In summary, we have investigated the static and dynamic response of a GaAs/(Ga,Al)As microdisk laser with IFQDs in the active region. Steady-state measurements of the stimulated emission yield a quality factor $Q \sim 6200$ and a coupling constant $\beta \sim 0.09$. The broad gain spectrum produces mode hopping between spectrally adjacent whispering gallery modes as a function of either temperature or excitation power. Time-resolved photoluminescence measurements show marked differences between the radiative decay rates in processed and unprocessed samples. Surprisingly, there is little difference between the dynamics of the emission from microdisks containing IFQDs and control samples without IFQDs. These microdisk lasers provide new templates for exploiting the interplay between 0D states and confined photons for quantum information processing.

This work was supported by the DARPA QuIST program, NSF-DMR and Sun Microsystems. We thank E. Hu for critical comments, and R. Epstein, O. Maksimov, and M. Stone for technical advice at various stages of this project.

* Electronic address: nsamarth@psu.edu

- ¹ A. Imamoglu, D. D. Awschalom, G. Burkard, D. P. DiVincenzo, D. Loss, M. Sherwin, and A. Small, Phys. Rev. Lett. **83**, 4204 (1999).
- ² P. Michler, A. Kiraz, C. Becher, W. V. Schoenfeld, P. M. Petroff, L.D. Zhang, E. Hu, A. Imamoglu, Science **290**, 2282 (2000).
- ³ D. K. Young, L. Zhang, D. D. Awschalom, and E. L. Hu, Phys. Rev. B **66**, 081307(R) (2002).
- ⁴ U. Mohideen, W. S. Hobson, S. J. Pearton, F. Ren, and R. E. Slusher, Appl. Phys. Lett. **64**, 1911 (1994).
- ⁵ K. J. Luo, J. Y. Xu, H. Cao, Y. Ma, S. H. Chang, S. T. Ho, and G. S. Solomon, Appl. Phys. Lett. **77**, 2304 (2000).
- ⁶ D. Gammon, E. S. Snow, and D. S. Katzer, Appl. Phys. Lett. **67**, 2391 (1995).
- ⁷ J. Hours, S. Varoutsis, M. Gallart, J. Bloch, I. Robert-Philip, A. Cavanna, I. Abram, F. Laruelle, and J. M. Gerard, Appl. Phys. Lett. **82**, 2206 (2003).
- ⁸ W. H Wang, S. Ghosh, F. Mendoza, D. D. Awschalom, and N. Samarth, (unpublished).
- ⁹ C. H. Henry, IEEE J. Quantum Electron. **QE-18**, 259 (1982).
- ¹⁰ G. Bjork, A. Karlsson, and Y. Yamamoto, Appl. Phys. Lett. **60**, 304 (1992).
- ¹¹ M. K. Chin, D. Y. Chu, and S. T. Ho, J. Appl. Phys. **75**, 3302 (1994).
- ¹² R. E. Slusher, A. F. J. Levi, U. Mohideen, S. L. McCall, S. J. Pearton, and R. A. Logan, Appl. Phys. Lett. **63**, 1310 (1993).
- ¹³ G. Bjork, A. Karlsson, and Y. Yamamoto, Phys. Rev. A **50**, 1675 (1994).
- ¹⁴ G. Bjork and Y. Yamamoto, IEEE J. Quantum Electron. **27**, 2386 (1991).
- ¹⁵ By definition, β and ξ are related by a proportionality factor. We have checked that the fit yields credible estimates for the physical parameters involved in this factor.
- ¹⁶ U. Mohideen, R. E. Slusher, F. Jahnke, and S. W. Koch, Phys. Rev. Lett. **73**, 1785 (1994).

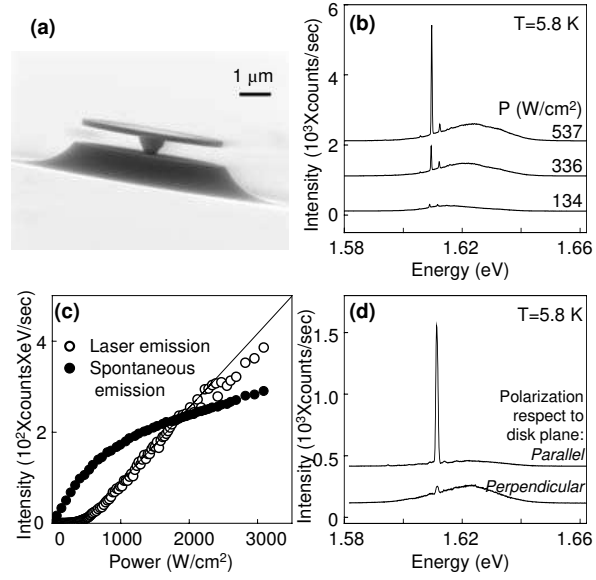


FIG. 1: (a) SEM image of microdisk laser structure. (b) Excitation power dependence of the emission spectrum of a single microdisk at $T = 5.8$ K. (c) Intensity of the stimulated emission (mode $TE_{35,1}$) and spontaneous emission vs. pump power. (d) Polarization-resolved far field emission from the side of a single microdisk. The top and the bottom spectra are polarization parallel and perpendicular to the disk plane, respectively.

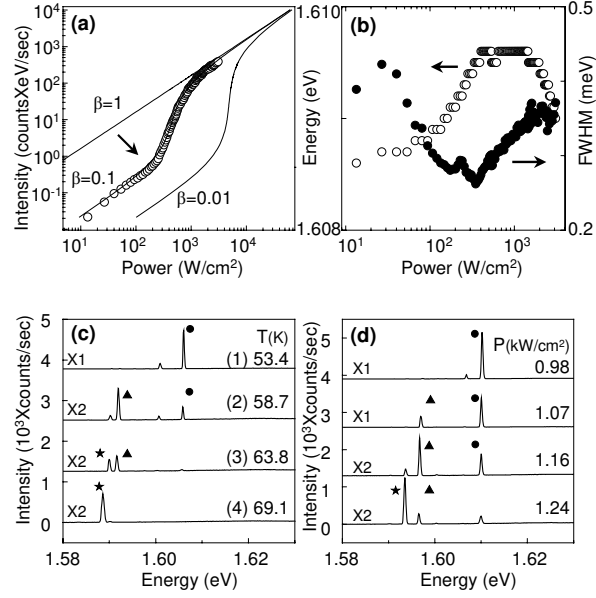


FIG. 2: (a) Power dependence of lasing intensity plotted on a log-log scale. The arrow indicates the laser threshold. Solid curves are based on equation (1) with coupling constant $\beta = 1, 0.1, 0.01$. (b) Power dependence of the energy (open circles) and width (solid circles) of the lasing mode. (c) Temperature dependence of microdisk emission spectrum, showing mode hopping between the TE_{35,1} (circle), TE_{30,2} (triangle) and TE_{26,3} (star) WGMs. (d) Pump power dependence of microdisk emission spectra at a sample mount temperature of $T = 5$ K.

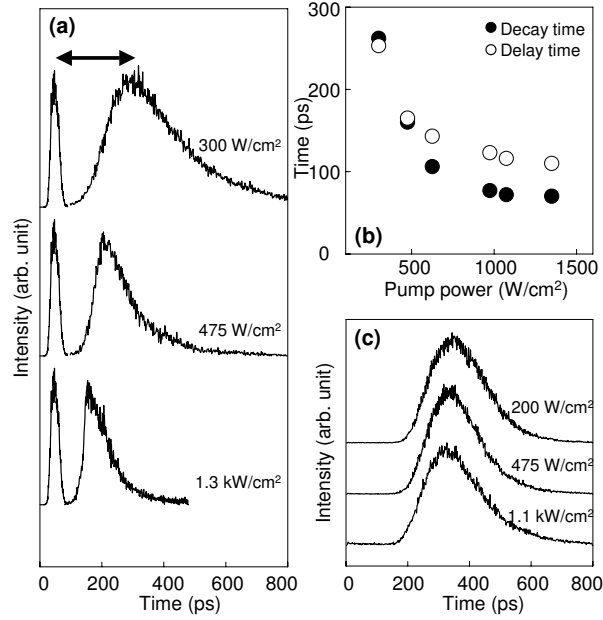


FIG. 3: (a) Temporal evolution of microdisk emission at 1.615 eV. Data at different pump intensities (indicated next to each spectrum) has been normalized and vertically shifted for clarity. The zero of time is fixed at the arrival of the excitation laser pulse (tuned to 1.676 eV). (b) Power dependence of decay and delay times. Decay time, defined as the 1/eth time constant of the decay tail, is determined from exponential fits to the data. Delay time is defined as the interval between the peaks of the excitation and microdisk emission pulses (arrow in (a)). Both show a marked decrease with increasing pump power. (c) The unprocessed part of the sample does not show any noticeable changes in either the pulse width or the delay time as input power is increased. All data in (a) - (c) are taken at 5 K.